*applied sciences*

MDPI

*Article*

# Charge Carrier Transport in Van Der Waals Semiconductor InSe Intercalated with $RbNO_3$ Probed by Direct Current Methods

**Zakhar R. Kudrynskyi [1,2,*], Illya V. Mintyanskii [2], Petro I. Savitskii [2] and Zakhar D. Kovalyuk [2]**

[1] Advanced Materials Research Group, Faculty of Engineering, The University of Nottingham, Nottingham NG7 2RD, UK
[2] I.M. Frantsevich Institute for Problems of Materials Science, National Academy of Sciences of Ukraine, Chernivtsi Branch, 58001 Chernivtsi, Ukraine; Mintyanskii.ipm@gmail.com (I.V.M.); chd.ipm@gmail.com (P.I.S.); zakhar.kovalyuk@gmail.com (Z.D.K.)
* Correspondence: zakhar.kudrynskyi@nottingham.ac.uk

**Abstract:** Layered van der Waals (vdW) semiconductors show great promise to overcome limitations imposed by traditional semiconductor materials. The synergistic combination of vdW semiconductors with other functional materials can offer novel working principles and device concepts for future nano- and optoelectronics. Herein, we investigate the influence of the intercalation of semiconducting *n*-type InSe vdW crystals with ferroelectric rubidium nitrate ($RbNO_3$) on the transport of charge carriers along and across the layers. The apparent maxima in the temperature dependences of the Hall coefficient are explained in the framework of a model that predicts, along with three-dimensional carriers, the existence of two-dimensional ones contributing only to the conductivity along the layers. The revealed increase of the conductivity anisotropy and its activation variation with temperature, which is mainly due to a decrease of the conductivity across the layers, confirm a two-dimensionalization of electron gas in n-InSe after insertion of the ferroelectric. From the numerical analysis, we determined the densities of carriers of both types, concentrations of donors and acceptors, as well as the value of the interlayer barrier.

**Keywords:** indium selenide; ferroelectric intercalation; Hall effect; conductivity anisotropy

**Citation:** Kudrynskyi, Z.R.; Mintyanskii, I.V.; Savitskii, P.I.; Kovalyuk, Z.D. Charge Carrier Transport in Van Der Waals Semiconductor InSe Intercalated with $RbNO_3$ Probed by Direct Current Methods. *Appl. Sci.* **2021**, *11*, 5181. https://doi.org/10.3390/app11115181

Academic Editor: Francesco Dell'Olio

Received: 3 May 2021
Accepted: 31 May 2021
Published: 2 June 2021

**Publisher's Note:** MDPI stays neutral with regard to jurisdictional claims in published maps and institutional affiliations.

**Copyright:** © 2021 by the authors. Licensee MDPI, Basel, Switzerland. This article is an open access article distributed under the terms and conditions of the Creative Commons Attribution (CC BY) license (https://creativecommons.org/licenses/by/4.0/).

## 1. Introduction

In recent years, the diverse family of layered van der Waals (vdW) crystals has been attracting a great deal of attention as a versatile material platform for fundamental and applied research [1–3]. The rapid development in this field has renewed interest in intercalation, which is a powerful approach to engineer the properties of layered materials [4,5]. The peculiarities of the crystalline structure of layered vdW crystals—namely, the absence of dangling bonds within a separate layer and large interlayer gaps (3–4 Å)—enable the properties of pristine crystals to be tailored by means of intercalation (i.e., by the insertion of various guest species between layers). In particular, intercalation could be used as an effective method to introduce new functionalities or enhance the existing parameters of a promising class of semiconducting vdW crystals known as metal monochalcogenides, such as InSe, GaSe, etc. In the pristine form, these crystals have recently emerged as an excellent material base not only for quantum science, but also for a wide range of innovative technologies, including quantum metrology, high broadband photosensors, light-emitting diodes, resonant tunnelling transistors with multiple regions of negative differential conductance, and field-effect transistors (FETs) with high electron mobility exceeding that of silicon-based FETs [6–16].

For layered InSe and GaSe crystals, intercalates with ferroelectric salts ($KNO_3$, $KNO_2$, $NaNO_2$, $RbNO_3$, etc.) form a wide group of insertion compounds [17–22]. The insertion of the salts into the crystal structure was confirmed by X-ray studies. In particular, the X-ray diffraction patterns of the InSe<$RbNO_3$> structure indicate the presence of InSe

and $RbNO_3$ phases and demonstrate the increase of the lattice parameter $c$ (along the crystallographic C axis) to 29.641 Å (for pristine InSe $c$ = 24.946 Å), while the in-plane lattice parameter $a$ remains unchanged [19]. Atomic force microscopy (AFM) imaging of the vdW surfaces of InSe and GaSe crystals after insertion of ionotronic salts revealed the presence of nanodimensional 3D inclusions of ferroelectric phases. For the GaSe<$RbNO_3$> structure, a pyramidal form was identified [17,20], whereas in the case of InSe<$RbNO_3$>, small islands of ionic salt were observed which created nanosized rings with an outer diameter less than 50 nm [18]. Their height did not exceed the width of vdW gap (~3.5 Å) and the surface density in the plane (0001) ranged between $10^9$ and $10^{10}$ $cm^{-2}$.

Photoconductivity spectra of InSe<$RbNO_3$> investigated in earlier studies [18] revealed significant photosensitivity at $h\nu < E_g$, which is higher than that in InSe single crystals. This was ascribed to the formation of a nanotextured interface between the ionic salt and layered crystal, as well as to the peculiarities of photoconductivity in anisotropic materials. The intercalation insertion of ferroelectric molecules into the interlayer space of III-VI semiconductors enables new mechanisms of charge accumulation, which is promising for the development of solid-state supercapacitors [17]. Thus, ferroelectric intercalating agents are promising materials for a wide range of applications, but little is known about their properties. Earlier ferroelectric nanocomposites obtained by exposing layered III-VI crystals to salt melts were investigated using AFM, X-ray photoelectron spectroscopy, optical absorption spectroscopy, etc. Although, the electrical properties of this hybrid semiconductor/ferroelectric system are interesting from both fundamental and practical points of view, so far they have only been studied by means of alternating current (a.c.) impedance spectroscopy methods [17,18]. In this paper, we report on the influence of ferroelectric rubidium nitrate ($RbNO_3$) intercalation on the electrical parameters of semiconducting $n$-type InSe vdW crystals and their anisotropy probed with direct current (d.c.) techniques.

## 2. Materials and Methods

In our study we used low-resistivity $n$-InSe single crystals grown by the Bridgman method from a non-stoichiometric melt $In_{1.03}Se_{0.97}$. From the obtained ingot we mechanically cleaved plane-parallel plates with shape suitable for measurements of Hall effect and conductivity in different crystallographic directions. After the electrical characteristics of the pristine samples were measured, samples were subjected to the insertion (intercalation) of a molecular guest component into the lattice by exposing the InSe samples to a melt of $RbNO_3$ at a temperature $T$ = 370 °C for 10 min. A porcelain crucible with the melt was placed in a hermetical box filled with air dried with phosphorus pentoxide ($P_2O_5$). The repeated intercalation was performed at the same technological conditions. To distinguish a possible effect of associated thermal treatment, other pristine samples were annealed in vacuum at the same time-temperature conditions.

Measurements of the temperature dependences of the conductivity along the layers $\sigma_{\perp C}$ and Hall coefficient $R_H$ were carried out for samples shaped as rectangular parallelepipeds with typical dimensions of 10 × 2.5 × 0.8 $mm^3$ with d.c. passing through the samples in a constant magnetic field. Note that the electrical characteristics for the pristine and intercalated compound were measured for the same sample, whereas the influence of vacuum annealing was established for other samples cleaved from neighboring parts of the ingot. For the pristine and annealed samples, we used indium as a contact material, and for the intercalated ones we used silver paste.

The mechanical properties of layered InSe crystals make it possible to cut samples with the prevailing dimension across the layers. That is why we used a four-probe method proposed in [23] to measure the conductivity component $\sigma_{\parallel C}$. In this case, the typical dimensions of samples were ~5 × 3 $mm^2$ (cleaved surface) with ~0.6 mm thickness. According to this method, a contact material was deposited onto cleaved surfaces perpendicular to the crystallographic C axis. The current contacts covered almost the whole surface of each cleaved side. Voltage was measured between a pair of small-area probe contacts which were located close to the current contacts. The spacing between the contacts on each

cleaved surface did not exceed 0.5 mm. This method is based on the assumptions that the voltage $U$ between the pair of the probe contacts does not differ significantly from the potential difference between the current ones, and that the current density through the sample is uniform. Later, this assumption was confirmed through a numerical analysis of the conductivity across the layers for samples with different $\sigma_{\perp C}/\sigma_{\parallel C}$ ratios at different sample dimensions and contacts to them [24]. Thus, this technique to measure $\sigma_{\parallel C}$ in crystals with high $\sigma_{\perp C}/\sigma_{\parallel C}$ anisotropy is sufficiently reliable, and was later applied in other studies [25–27].

The measurements of "vertical" conductivity were carried out for the samples cleaved from neighboring parts of the same ingot as the samples for investigations of electrical parameters along the layers. These measurements were carried out only in the temperature range 80 to 300 K. Higher temperatures were not used in order to avoid the decomposition of planar interlayer aggregates of defects.

## 3. Results and Discussion

### *3.1. Transport Properties along the Layers*

Temperature dependences of the conductivity $\sigma_{\perp C}$ and Hall mobility of electrons $\mu_{\perp C}$ along the layers, as well as those of the Hall coefficient $R_H$ for the pristine, vacuum annealed, and $RbNO_3$-intercalated InSe crystals are shown in Figures 1–3. Numerical values of the parameters at 80 and 300 K are listed in Table 1. It is established that for the pristine sample, the Hall coefficient decreases approximately twice with increasing temperature from 80 to 300 K. Such dependence is caused by a slight variation of the electron concentration—a shallow donor level (18.5 meV) is preferably ionized already at 80 K, while the deeper donors still do not manifest. It is generally accepted that in undoped InSe crystals, the shallow donor is related to interstitial indium atoms $In_i$ [28]. A decrease in the mobility component with increasing temperature within the investigated range is caused by the interaction of electrons with optical phonons, which is the dominant scattering mechanism [29,30]. Such behavior of $R_H$ and $\mu_{\perp C}$ defines a metallic character of the conductivity $\sigma_{\perp C}$ variation at $T < 370$ K (Figure 1). Only at higher temperatures does the activation of electrons from a deeper donor rapidly increase, resulting in the transition to $\sigma_{\perp C}$ $(T)$ dependence which is typical for semiconductors.

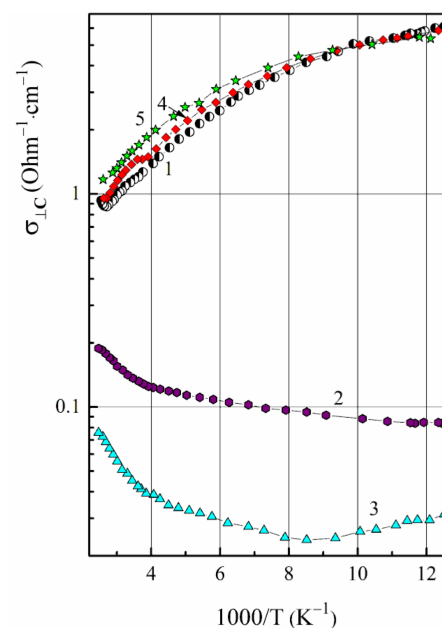


**Figure 1.** Temperature dependences of conductivity along the layers for the *n*-InSe samples: pristine (1), first-time and repeatedly intercalated with $RbNO_3$ (2 and 3, respectively), and annealed in vacuum (4 and 5, respectively).

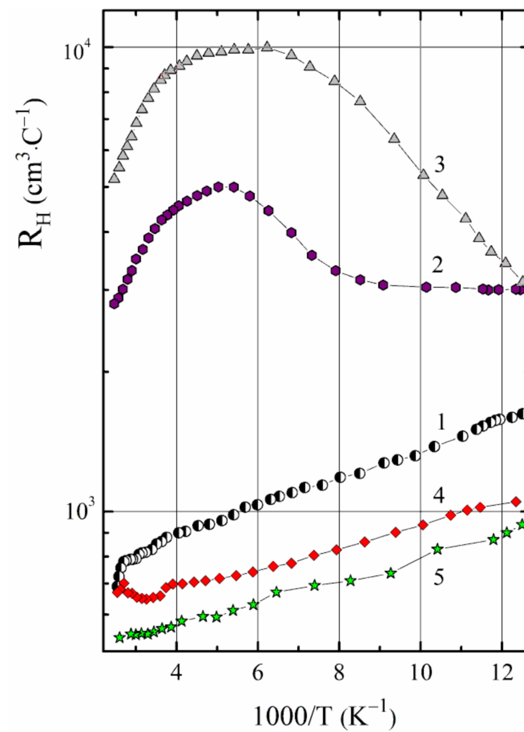


**Figure 2.** Temperature dependences of the Hall coefficient for the *n*-InSe samples: pristine (1), first-time and repeatedly intercalated with $RbNO_3$ (2 and 3, respectively), and annealed in vacuum (4 and 5, respectively).

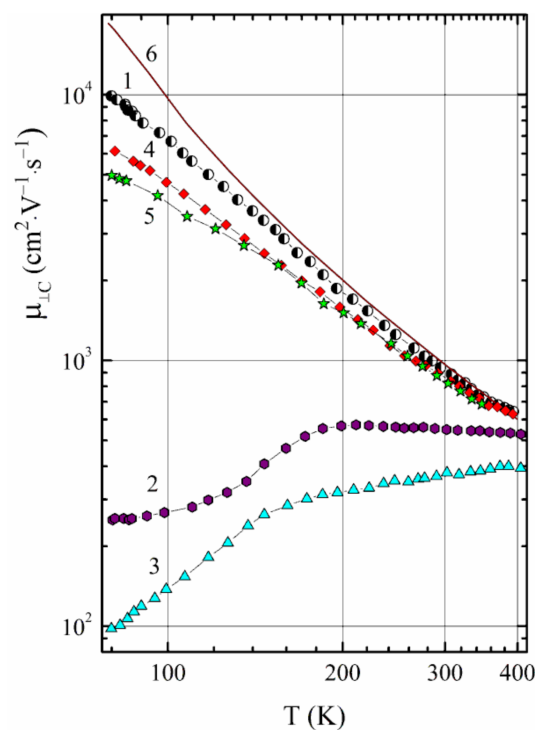


**Figure 3.** Temperature dependences of the Hall mobility along the layers for the *n*-InSe samples: pristine (1), first-time and repeatedly intercalated with $RbNO_3$ (2 and 3, respectively), and annealed in vacuum (4 and 5, respectively). Curve 6 shows drift mobility calculated according to the model in [25,26].

**Table 1.** Electrical parameters along the layers of different $n$-InSe samples.

| Sample | $\sigma_{\perp C}$ (Ohm$^{-1}$·cm$^{-1}$) 80 K | $\sigma_{\perp C}$ (Ohm$^{-1}$·cm$^{-1}$) 300 K | $n$ (cm$^{-3}$) 80 K | $n$ (cm$^{-3}$) 300 K | $\mu_{\perp C}$ (cm·V$^{-1}$·s$^{-1}$) 80 K | $\mu_{\perp C}$ (cm·V$^{-1}$·s$^{-1}$) 300 K |
|---|---|---|---|---|---|---|
| 1 | 6.10 | 1.121 | $3.85 \times 10^{15}$ | $7.61 \times 10^{15}$ | 9905 | 919 |
| 2 | 0.0837 | 0.142 | $2.08 \times 10^{15}$ | $1.61 \times 10^{15}$ | 251.3 | 549 |
| 3 | 0.0313 | 0.0487 | $2.00 \times 10^{15}$ | $8.04 \times 10^{14}$ | 97.9 | 378 |
| 4 | 5.91 | 1.328 | $5.93 \times 10^{15}$ | $9.60 \times 10^{15}$ | 6226 | 864 |
| 5 | 4.72 | 1.531 | $6.66 \times 10^{15}$ | $1.14 \times 10^{16}$ | 4970 | 836 |

According to the theoretical model in [29,30], the scattering of carriers with homopolar optical phonons, which are polarized along the crystallographic C axis and modulate the thickness of a separate layer, is dominant in layered crystals. In this case, the relaxation time $\tau_{FS}$ is given by:

$$1/\tau_{FS} = 2g^2\omega\left[((\varepsilon/\hbar\omega)+1)^{\frac{1}{2}}\,n_{ph} + \left(n_{ph}+1\right)\theta(\varepsilon-\hbar\omega)((\varepsilon/\hbar\omega)-1))^{\frac{1}{2}}\right] \quad (1)$$

Here, $g^2 = \mathcal{E}_0^2 m^{*\frac{3}{2}} MN\hbar(\hbar\omega)^{\frac{3}{2}}$ is the electron–phonon coupling constant, $\hbar\omega$ is the phonon energy, $\mathcal{E}_0$ is the deformation potential, $M$ is the reduced ionic mass of the phonon mode, $N$ is the number of cells per unit volume, $\varepsilon$ is the electron energy, $n_{ph} = [\exp(\hbar\omega/kT)-1]^{-1}$ is the phonon occupation number, $m^* = \left(m^{*2}_{\perp C} m^*_{\parallel C}\right)^{1/3}$ is the density-of-states effective mass, and $\theta(x) = 1$ at $x \geq 0$ and 0 at $x < 0$. The drift mobility along the layers caused by this scattering mechanism is:

$$\mu_{FS} = e < \tau_{FS} > /m^* \quad (2)$$

In the three-dimensional approximation of the scattering with the homopolar optical phonon $A'_{1g}$ ($\hbar\omega = 14.3$ мeB) and $g^2 = 0.056$, the $\mu_{FS}(T)$ dependence follows the pattern shown by curve 6 in Figure 3. The difference between the $\mu_{FS}(T)$ and apparent mobility dependence for the pristine sample can be explained by the effect of additional scattering with ionized impurities. Thus, the total mobility is $\mu^{-1} = \mu_{FS}{}^{-1} + \mu_{BH}{}^{-1}$, where $\mu_{BH}$ is the Brooks–Herring mobility for scattering with ionized impurities. Assuming that in the Brooks–Herring expression the effective concentration of screening carriers is equal to the concentration of free electrons, for the pristine sample we obtain the concentration of ions to be $N_i = 7.35 \times 10^{15}$ cm$^{-3}$, and that of compensating acceptors to be $N_A = (N_i - n)/2 = 1.94 \times 10^{15}$ cm$^{-3}$. This means that the pristine InSe crystal is not a highly compensated semiconductor.

The main peculiarities of the intercalated crystals are the presence of extrema in the temperature dependences of $R_H$ and non-monotonous changes of $\mu_{\perp C}$. In comparison to the pristine $n$-InSe sample, the Hall coefficient for the intercalated ones is higher. Starting from 80 K for sample 2 and after 110 K for sample 3, the $R_H$ values increase with temperature and take their maxima at 160 and 200 K, respectively. The low-temperature mobility of electrons along the layers becomes decreased after the first-time and repeated insertion of $RbNO_3$. For both intercalated samples, the mobility increases with increasing temperature and, in the high-temperature range, is nearly the same as in pristine samples. It should be noted that during the insertion of the ionic salt between the layers of $n$-InSe, the samples are simultaneously subjected to thermal annealing, as the intercalation is done at high temperatures. Usually, a vacuum treatment at 450–550 °C results in an increase of free carriers because of the dissociation of interlayer In inclusions that continues for 2 h [26]. However, at the conditions used for the intercalation (low temperature and duration), the effect of annealing on the electrical parameters is not determinative.

The obtained dependences of the electrical characteristics for the intercalated crystals are typical for transport properties with two types of charge carriers contributing to the total conductivity $\sigma = \sigma_2 + \sigma_3$, with corresponding concentrations and essentially different

mobilities. Within such a model, the Hall coefficient is given as a function of carrier concentration and mobility by the following expression:

$$R_H = \frac{r_2 n_2 \mu_2^2 + r_3 n_3 \mu_3^2}{e(n_2 \mu_2 + n_3 \mu_3)^2} \quad (3)$$

Here $r_2$, $n_2$, $\mu_2$ and $r_3$, $n_3$, $\mu_3$ are Hall factors, concentrations, drift, and Hall mobilities for two types of electrons. Assuming that $r_2 = r_3 = 1$ and the total concentration of electrons is constant ($n_2 + n_3$ = const), the parameter $R_H$ reaches its maximum when the conductivities are the same ($\sigma_2 = \sigma_3$).

According to the literature [31–33], extrema in $R_H(T)$ dependences were observed in many compounds and were explained by a simultaneous contribution to the conductivity of the carriers from a main band and an impurity band, which is separated from it, with essentially different mobilities. However, the apparent mobility values are too high to be attributed to an impurity band, which is evidence against such an explanation in our case.

A mixed conductivity of the samples under investigation could also be caused by light and heavy electrons in the conduction band. However, starting from band structure calculations for $\gamma$-InSe [34], a model of a complex conduction band should be rejected.

The decrease of the Hall coefficient with decreasing temperature could also be explained as a tendency to change the conductivity type from *n* to *p*. However, a self-compensation mechanism is inherent for *n*-InSe crystals—that is, adding acceptors leads to the appearance of new compensating donors. Besides, it is known that even if the impurities are acceptors within a layer, they act as donors in the interlayer positions [35]. Therefore, this explanation of the Hall coefficient behavior after the insertion of $RbNO_3$ is probably not correct.

As we found earlier [36–39], non-monotonic temperature dependences of $R_H$ and $\mu_{\perp C}$ in *n*-InSe irradiated with electrons can be explained assuming that electron transport along the layers is due to a contribution of high-mobility three-dimensional (3D) electrons and less-mobile two-dimensional (2D) ones. It is known that polytypism and vdW coupling between the InSe layers cause the presence of typical planar stacking faults between different structure polytypes, where impurities (dopants, intercalants, intrinsic atoms, residual impurities) can be accumulated. The presence of degenerate 2D accumulating layers is ascribed to planar inclusions of charged donor impurities at such stacking faults. Their electrical potential bends the c-band bottom, creating energy wells across the layers. In such energy sub-bands, electrons behave as a degenerate 2D electron gas—that is, they keep free motion along the layers but are restricted to move across them.

The apparent temperature dependences of the Hall coefficient and mobility for the intercalated samples can also be interpreted within the model that takes into account the contributions of 3D and 2D electrons to the transport of charge carriers along the layers. One can assume that 2D carriers largely determine the transport properties at low temperatures. With increasing temperature, the 2D carriers become thermally activated in the main bulk of *n*-InSe and the dimensionality of electron transport changes.

If we assume that, according to [40], the dependence of the mobility ratio $b = \mu_3/\mu_2$ on temperature is much weaker than that on the concentration ratio of 3D and 2D electrons $x = n_3/n_2$, then in the maximum point of the Hall coefficient the equation

$$R_{max}/R_{dep} = (b+1)^2/4b \quad (4)$$

is correct. Here, $R_{max}$ is the value of the parameter at the depletion of carriers when $n_{dep} = n_2 + n_3$ = const. Knowing the value of $b$, one can determine from the experimental data the values of $n_2$ and $n_3$ as a function of temperature using expression (3). For the intercalated sample 3, calculations were not done because it is impossible to determine $n_{dep}$, but for sample 2 at $r_2 = r_3 = 1$ and $n_{dep} = 2.08 \cdot 10^{15}$ cm$^{-3}$ the temperature dependences of the concentrations are shown in Figure 4.

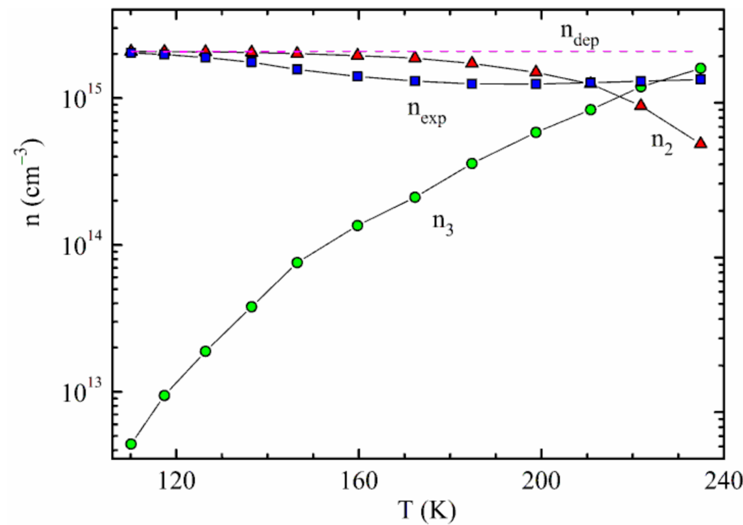


**Figure 4.** Temperature dependences of the experimental and calculated (2D and 3D) concentrations. $n_{\text{dep}}$ is the concentration of depletion.

Further analysis of the $n_3(T)$ dependence was carried out within a "single donor–single acceptor" model considering that $N_D - N_A = n_{\text{dep}}$. From the temperature dependence of the Fermi level, which for a parabolic c-band is related with the concentration of the carriers as

$$n_C = 4\pi \left( \frac{2m^* kT}{h^2} \right)^{3/2} F_{1/2}\left( \frac{\mu}{kT} \right), \quad (5)$$

the Fermi integral was calculated, and the chemical potential was determined for a set of temperature points. With the significant compensation of donors, the following equation takes place:

$$\mu = kT \ln \frac{N_D - N_A}{N_C + gN_A e^{E_D/kT}} \quad (6)$$

This equation contains two unknown parameters, $N_D$ and $E_D$, related by the expression:

$$N_A = \frac{n_{dep} - N_C e^{\mu/kT}}{g e^{\frac{\mu + E_D}{kT}}} \quad (7)$$

By taking the spin degeneracy factor to be $g$ = 2 and writing the expression for $N_\text{A}$ at two significantly different temperatures, we obtain a corresponding difference equation that contains the only unknown parameter $E_D$, which is obtained from a fitting procedure. Thus, for the intercalated sample 2 we obtain that $E_D$ = 90.4 meV, $N_D = 5.38 \cdot 10^{15}$ cm$^{-3}$, and $N_A = 3.30 \cdot 10^{15}$ cm$^{-3}$. Note that in our case $E_D$ is the depth of the potential well and its value is close to those observed in [36] (0.09–0.14 eV).

To define the nature of the additional interlayer defects which appeared after the insertion of $RbNO_3$, it is necessary to carry out detailed studies. Here, we assume that the intercalation leads to the formation of additional interlayer planar defects and potential wells. For such samples, one can expect a decrease in the "vertical" conductivity and high values for the anisotropy ratio at low temperatures.

### 3.2. Conductivity Anisotropy

Temperature dependences of the conductivity across the layers $\sigma_{\parallel C}$ and the conductivity anisotropy $\sigma_{\perp C}/\sigma_{\parallel C}$ for the pristine, intercalated with $RbNO_3$, and vacuum annealed crystals of InSe are shown in Figures 5 and 6, and the numerical values of the parameters are listed in Table 2. The transversal conductivity component is essentially smaller than the longitudinal one for all the samples. Thermal treatment in vacuum causes a slight

increase of $\sigma_{||C}$ and a decrease in the anisotropy. Note that for the pristine and annealed samples, there are only slight variations of $\sigma_{||C}$ and $\sigma_{\perp C}/\sigma_{||C}$ with temperature. On the contrary, the insertion of $RbNO_3$ leads to a significant (by a factor of 80 to 800) decrease in the $\sigma_{||C}$ component, and $\sigma_{\perp C}/\sigma_{||C}$ considerably increases at 80 K (by a factor of 10 to 40) and exponentially decreases with increasing temperature with a higher slope. The increased anisotropy values are mainly because of the decreased transversal conductivity.

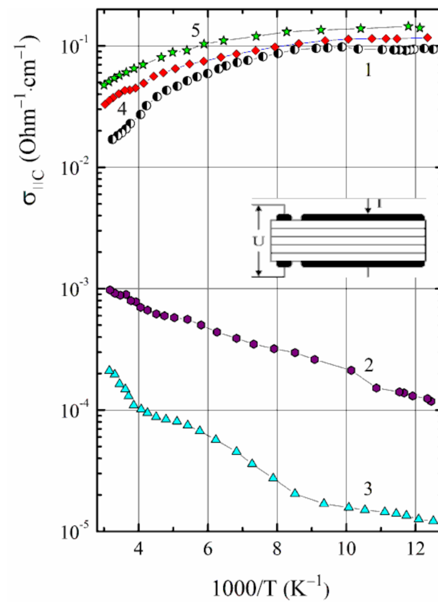


**Figure 5.** Temperature dependences of the transversal conductivity for the *n*-InSe samples: pristine (1), first-time and repeatedly intercalated with $RbNO_3$ (2 and 3, respectively), and annealed in vacuum (4 and 5, respectively). Inset shows the geometry of sample contacts for measurements of $\sigma_{||C}$.

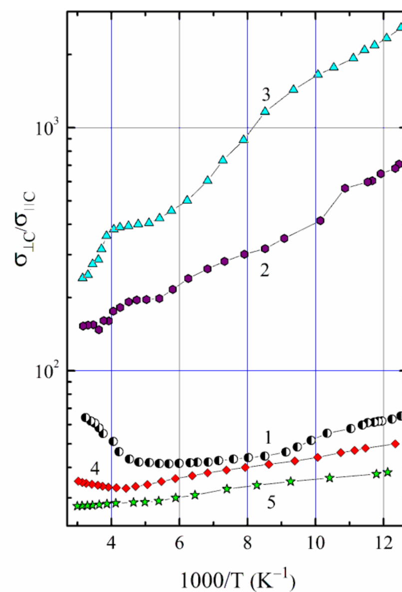


**Figure 6.** Temperature dependences of the conductivity anisotropy for the *n*-InSe samples: pristine (1), first-time and repeatedly intercalated with $RbNO_3$ (2 and 3, respectively), and annealed in vacuum (4 and 5, respectively).

**Table 2.** Conductivity across the layers and conductivity anisotropy for different samples of $n$-InSe.

| Sample | $\sigma_{\parallel C}$ ($Ohm^{-1}\cdot cm^{-1}$) 80 K | 300 K | $\sigma_{\perp C}/\sigma_{\parallel C}$ 80 K | 300 K | $\Delta E_b$ (meV) | A |
|---|---|---|---|---|---|---|
| 1 | 0.09375 | 0.01826 | 65.1 | 62.1 | 7.6 | 21.7 |
| 2 | $1.183 \times 10^{-4}$ | $9.88 \times 10^{-4}$ | 708 | 154 | 15.3 | 77.5 |
| 3 | $1.218 \times 10^{-5}$ | $1.964 \times 10^{-4}$ | 2575 | 248 | 23.1 | 97.0 |
| 4 | 0.1182 | 0.0387 | 50.0 | 34.3 | 4.6 | 25.9 |
| 5 | 0.1367 | 0.0549 | 38.8 | 27.9 | 3.5 | 234 |

Although many properties of InSe (e.g., mechanical) are highly anisotropic, it is not because of the material's band structure. It is known that the energy bands forming the fundamental absorption edge of InSe are created with the significant participation of the $p_z$-orbitals of Se, and that they have 3D character [34]. Taking into account that for $n$-InSe the longitudinal component of the effective mass is higher than the transversal one ($m^*_{\perp C} = 0.13m_0$ and $m^*_{\parallel C} = 0.08m_0$ [41]), in an ideal case of the same averaged relaxation time along and across the layers one can expect the anisotropy ratio to be independent of the temperature, and to be less than 1. Thus, the apparent high conductivity anisotropy should be considered as defect-induced. A low energy of a longitudinal shift of the layers relative to each other leads to disordering in the sequence of layers and the creation of energy barriers between the $n$-InSe layers, which explains the anomalously high values of $\sigma_{\perp C}/\sigma_{\parallel C}$. To participate in conductivity across the layers, charge carriers should be activated over such barriers or tunnel through them.

Considering that the conductivity along the layers is

$$\sigma_{\perp C} = en\mu_{\perp C}, \tag{8}$$

and assuming that the conductivity across the layers occurs because of thermal activation of the carriers over the energy barrier $\Delta E_b$, in a one-dimensional model:

$$\sigma_{\parallel C} = en\mu_{\parallel C} exp(-\Delta E_b/kT), \tag{9}$$

and therefore the conductivity anisotropy in the low-temperature range is:

$$\sigma_{\perp C}/\sigma_{\parallel C} = Aexp(\Delta E_b/kT) \tag{10}$$

At the same averaged relaxation times, the pre-exponential factor $A = \mu_{\perp C}/\mu_{\parallel C} = m^*_{\parallel C}/m^*_{\perp C}$.

For the pristine $n$-InSe sample, the value of the energy barrier is small and is equal to 7.6 meV. Some decrease of the value after vacuum annealing is caused primarily by the increase of the transversal component: high temperature leads to the dissipation of interlayer inclusions, the concentration of interstitial donors increases, and their ionization increases $\sigma_{\parallel C}$. On the contrary, for the intercalated crystals we find a significant increase in $\Delta E_b$ (Table 2). However, for all the samples, the values of the pre-exponential factor ($A \approx 20 \div 100$) obviously do not correspond to the effective mass ratio, as it is not below 1 ($m^*_{\parallel C}/m^*_{\perp C}$ = 0.615). According to [25,27,42], high conductivity anisotropy of indium monoselenide is not related to a highly anisotropic scattering mechanism, but is caused by the presence of a significant concentration of 2D electrons, which do not participate in charge transfer across the layers, in contrast to 3D carriers. Within this model, expression (8) takes the form

$$\sigma_{\perp C} = e(n_2\mu_{2\perp C} + n_3\mu_{3\perp C}), \tag{11}$$

and the anisotropy depends on the relative value of the concentrations of 2D and 3D electrons and corresponding mobilities:

$$\frac{\sigma_{\perp C}}{\sigma_{\| C}} = \frac{n_2\mu_{2\perp C} + n_3\mu_{3\perp C}}{n_3\mu_{3\| C}} exp(\Delta E_b/kT). \quad (12)$$

Because of the limitations of the available experimental data, it is impossible to determine the separate mobility components contained in Equation (12). However, taking into account the high values of the preexponential factor, we can assume that 2D carriers are dominant.

## 4. Conclusions

InSe vdW crystals intercalated with ferroelectric $RbNO_3$ are characterized by non-monotonic temperature dependences of the Hall coefficient and Hall mobility along the layers. They can be explained in the framework of a model which predicts, along with high-mobility 3D electrons, the presence of less-mobile 2D ones which do not participate in charge transport across the layers. The two-dimensionalization of electron gas found after the insertion of the ferroelectric salt into *n*-type InSe agrees with the significant increase in the conductivity anisotropy and its exponential variation with temperature. It should be noted that the increase in the anisotropy ratio $\sigma_{\perp C}/\sigma_{\| C}$ is mainly caused by a decrease of the transversal conductivity component.

**Author Contributions:** Conceptualization, Z.R.K. and Z.D.K.; methodology, I.V.M., P.I.S. and Z.D.K.; software, P.I.S.; validation, Z.R.K. and Z.D.K.; formal analysis, Z.R.K., I.V.M. and P.I.S.; investigation, Z.R.K., I.V.M. and P.I.S.; resources, Z.R.K. and Z.D.K.; data curation, I.V.M. and P.I.S.; writing—original draft preparation, Z.R.K., I.V.M. and P.I.S.; writing—review and editing, Z.R.K., I.V.M., P.I.S. and Z.D.K.; supervision, Z.D.K.; project administration, Z.D.K.; funding acquisition, Z.D.K. All authors have read and agreed to the published version of the manuscript.

**Funding:** This research was funded by the National Academy of Sciences of Ukraine.

**Institutional Review Board Statement:** Not applicable.

**Informed Consent Statement:** Not applicable.

**Conflicts of Interest:** The authors declare no conflict of interest.

## References

1. Duong, D.L.; Yun, S.J.; Lee, Y.H. van der Waals layered materials: Opportunities and challenges. *ACS Nano* **2017**, *11*, 11803–11830. [CrossRef] [PubMed]
2. Di Bartolomeo, A. Emerging 2D materials and their van der Waals heterostructures. *Nanomaterials* **2020**, *10*, 579. [CrossRef] [PubMed]
3. Geim, A.K.; Grigorieva, I.V. Van der Waals heterostructures. *Nature* **2013**, *499*, 419–425. [CrossRef]
4. Stark, M.S.; Kuntz, K.L.; Martens, S.J.; Warren, S.C. Intercalation of layered materials from bulk to 2D. *Adv. Mater.* **2019**, *31*, 1808213. [CrossRef] [PubMed]
5. Rajapakse, M.; Karki, B.; Abu, U.O.; Pishgar, S.; Musa, M.R.K.; Riyadh, S.M.S.; Yu, M.; Sumanasekera, G.; Jasinski, J.B. Intercalation as a versatile tool for fabrication, property tuning, and phase transitions in 2D materials. *NPJ 2D Mater. Appl.* **2021**, *5*, 30. [CrossRef]
6. Kudrynskyi, Z.R.; Bhuiyan, M.A.; Makarovsky, O.; Greener, J.D.G.; Vdovin, E.E.; Kovalyuk, Z.D.; Cao, Y.; Mishchenko, A.; Novoselov, K.S.; Beton, P.H.; et al. Giant quantum hall plateau in graphene coupled to an InSe van der Waals crystal. *Phys. Rev. Lett.* **2017**, *119*, 157701. [CrossRef] [PubMed]
7. Bhuiyan, M.A.; Kudrynskyi, Z.R.; Mazumder, D.; Greener, J.D.G.; Makarovsky, O.; Mellor, C.J.; Vdovin, E.E.; Piot, B.A.; Lobanova, I.I.; Kovalyuk, Z.D.; et al. Photoquantum Hall effect and light-induced charge transfer at the interface of graphene/inse heterostructures. *Adv. Funct. Mater.* **2019**, *29*, 1805491. [CrossRef]
8. Mudd, G.W.; Svatek, S.A.; Hague, L.; Makarovsky, O.; Kudrynskyi, Z.R.; Mellor, C.J.; Beton, P.H.; Eaves, L.; Novoselov, K.S.; Kovalyuk, Z.D.; et al. High broad-band photoresponsivity of mechanically formed InSe–graphene van der waals heterostructures. *Adv. Mater.* **2015**, *27*, 3760–3766. [CrossRef]
9. Balakrishnan, N.; Kudrynskyi, Z.R.; Smith, E.F.; Fay, M.W.; Makarovsky, O.; Kovalyuk, Z.D.; Eaves, L.; Beton, P.H.; Patanè, A. Engineering p − n junctions and bandgap tuning of InSe nanolayers by controlled oxidation. *2D Mater.* **2017**, *4*, 025043. [CrossRef]

10. Balakrishnan, N.; Kudrynskyi, Z.R.; Fay, M.W.; Mudd, G.W.; Svatek, S.A.; Makarovsky, O.; Kovalyuk, Z.D.; Eaves, L.; Beton, P.H.; Patanè, A. Room temperature electroluminescence from mechanically formed van der Waals III–VI homojunctions and heterojunctions. *Adv. Opt. Mater.* **2014**, *2*, 1064–1069. [CrossRef]
11. Velichko, A.V.; Kudrynskyi, Z.R.; Paola, D.M.D.; Makarovsky, O.; Kesaria, M.; Krier, A.; Sandall, I.C.; Tan, C.H.; Kovalyuk, Z.D.; Patanè, A. Highly-mismatched InAs/InSe heterojunction diodes. *Appl. Phys. Lett.* **2016**, *109*, 182115. [CrossRef]
12. Kudrynskyi, Z.R.; Kovalyuk, Z.D. Photosensitive anisotype n-ZnSe/p-InSe and n-ZnSe/p-GaSe heterojunctions. *Tech. Phys.* **2014**, *59*, 1205–1208. [CrossRef]
13. Kudrynskyi, Z.; Khomyak, V.; Katerynchuk, V.; Kovalyuk, M.; Netyaga, V.; Kushnir, B. Fabrication and characterization of photosensitive n-ZnO/p-InSe heterojunctions. *Thin Solid Films* **2015**, *582*, 253–257. [CrossRef]
14. Ubrig, N.; Ponomarev, E.; Zultak, J.; Domaretskiy, D.; Zólyomi, V.; Terry, D.; Howarth, J.; Gutiérrez-Lezama, I.; Zhukov, A.; Kudrynskyi, Z.R.; et al. Design of van der Waals interfaces for broad-spectrum optoelectronics. *Nat. Mater.* **2020**, *19*, 299–304. [CrossRef]
15. Kudrynskyi, Z.R.; Kerfoot, J.; Mazumder, D.; Greenaway, M.T.; Vdovin, E.E.; Makarovsky, O.; Kovalyuk, Z.D.; Eaves, L.; Beton, P.H.; Patanè, A. Resonant tunnelling into the two-dimensional subbands of InSe layers. *Commun. Phys.* **2020**, *3*, 16. [CrossRef]
16. Bandurin, D.A.; Tyurnina, A.V.; Yu, G.L.; Mishchenko, A.; Zolyomi, V.; Morozov, S.V.; Kumar, R.K.; Gorbachev, R.V.; Kudrynskyi, Z.R.; Pezzini, S.; et al. High electron mobility, quantum Hall effect and anomalous optical response in atomically thin InSe. *Nat. Nanotechnol.* **2017**, *12*, 223–227. [CrossRef]
17. Bakhtinov, A.P.; Vodopyanov, V.N.; Kudrynskyi, Z.R.; Kovalyuk, Z.D.; Netyaga, V.V.; Lytvyn, O.S. Nanocomposite structures grown by inserting ionic salt $RbNO_3$ into van der Waals gaps of III−VI compound layered semiconductors. *Solid State Ionics* **2015**, *273*, 59–65. [CrossRef]
18. Bakhtinov, A.P.; Vodopyanov, V.N.; Ivanov, V.I.; Tkachuk, I.G.; Netyaga, V.V.; Savitskii, P.I.; Kovalyuk, Z.D. Impedance and photosensitivity spectra of nanocomposite structures based on layered semiconductor InSe and ionic salt $RbNO_3$. *Phys. Status Solidi A* **2018**, *24*, 1800460. [CrossRef]
19. Kudrynskyi, Z.R.; Netyaga, V.V. Nanocomposite material based on GaSe and InSe layered crystals intercalated by $RbNO_3$ ferroelectric. *J. Nano Electron. Phys.* **2013**, *5*, 03028.
20. Kovalyuk, Z.D.; Boledzyuk, V.B.; Pyrlya, M.M.; Potsiluiko, R.L.; Netyaga, V.V. The effect of the thermal introduction of $NaNO_2$ on the optical properties of indium and gallium monoselenides. *Phys. Chem. Solid State* **2016**, *17*, 544–547. [CrossRef]
21. Bakhtinov, A.P.; Vodopyanov, V.N.; Kovalyuk, Z.D.; Netyaga, V.V.; Konoplyanko, D.Y. Carrier transport in layered semiconductor (p-GaSe)–ferroelectric ($KNO_3$) composite nanostructures. *Semiconductors* **2011**, *45*, 338–349. [CrossRef]
22. Grigorchak, I.I.; Netyaga, V.V.; Kovalyuk, Z.D. On some physical properties of InSe and GaSe semiconducting crystals intercalated by ferroelectrics. *J. Phys. Condens. Matter.* **1997**, *9*, L191–L195. [CrossRef]
23. Pomer, F.; Bonet, X.; Segura, A.; Chevy, A. Electrical conductivity anisotropy in tin-doped n-type indium selenide. *Phys. Status Solidi B* **1988**, *145*, 261–268. [CrossRef]
24. Pomer, F.; Navasquillo, J. A method for measuring the resistivity of a layered semiconductor perpendicular to the layers. *Phys. Status Solidi A* **1988**, *110*, 585–592. [CrossRef]
25. Martinez-Pastor, J.; Segura, A.; Chevy, A. High temperature behavior of impurities and dimensionality of the charge transport in not purposely doped and tin doped indium selenide. *J. Appl. Phys.* **1993**, *74*, 3231–3237. [CrossRef]
26. Savitskii, P.I.; Mintyanskii, I.V.; Kovalyuk, Z.D. Annealing effect on conductivity anisotropy in indium selenide single crystals. *Phys. Status Solidi A* **1996**, *155*, 451–460. [CrossRef]
27. Riera, J.; Segura, A.; Chevy, A. Electrical resistivity anisotropy of silicon-doped n-indium selenide. *Phys. Status Solidi A* **1993**, *136*, K47–K50. [CrossRef]
28. Segura, A.; Wünstel, K.; Chevy, A. Investigation of impurity levels in *n*-type indium selenide by means of Hall effect and deep level transient spectroscopy. *Appl. Phys. A* **1983**, *31*, 139–145. [CrossRef]
29. Fivaz, R.C. Dimensionality and the electron-phonon interaction in layer structures. *Nuovo Cim. B* **1969**, *63*, 10–28. [CrossRef]
30. Schmid, P. Electron-lattice interaction in layered semiconductors. *Nuovo Cim. B* **1974**, *21*, 258–270. [CrossRef]
31. Essaleh, L.; Wasim, S.M.; Galibert, J. Effect of impurity band conduction on the electrical characteristics of n-type $CuInSe_2$. *J. Appl. Phys.* **2001**, *90*, 3993–3997. [CrossRef]
32. Laiho, L.; Lashkul, A.V.; Lahderanta, E.; Nedeoglo, D.D.; Nedeoglo, N.D.; Shakhov, M.A. Shallow donor states of Ag impurity in ZnSe single crystals. *Semicond. Sci. Technol.* **2006**, *21*, 654–660. [CrossRef]
33. Arushanov, E.; Schön, J.H.; Matsushita, H.; Takizawa, T. Impurity band in p-type $CuInSe_2$. *Phys. Status Solidi A* **1999**, *176*, 1009–1016. [CrossRef]
34. Gomes da Costa, P.; Dandrea, R.G.; Wallis, R.F.; Balkanski, M. First-principle study of electronic structure of $\gamma$-InSe and $\beta$-InSe. *Phys. Rev. B* **1993**, *48*, 14135–14141. [CrossRef]
35. Segura, A.; Martinez-Tomas, M.C.; Mari, B.; Casanovas, A.; Chevy, A. Acceptor levels in indium selenide. An investigation by means of the Hall effect, deep-level-transient spectroscopy and photoluminescence. *Appl. Phys. A* **1987**, *44*, 249–260. [CrossRef]
36. Mintyanskii, I.V.; Savitskii, P.I.; Kovalyuk, Z.D. Two-band conduction in electron-irradiated n-InSe single crystals. *Phys. Status Solidi B* **2015**, *252*, 346–356. [CrossRef]
37. Kovalyuk, Z.D.; Mintyanskii, I.V.; Savitskii, P.I. Effect of electron irradiation on conductivity anisotropy in n-InSe. *J. Nano Electron. Phys.* **2017**, *9*, 06013. [CrossRef]

38. Mintyanskii, I.V.; Savitskii, P.I.; Kovalyuk, Z.D.; Maslyuk, V.T.; Megela, I.G. Effect of the electron irradiation on electrical properties of n-InSe and their anisotropy. *Nuclear Phys. At. Energy* **2018**, *19*, 136–144. [CrossRef]
39. Mintyanskii, I.V.; Savitskii, P.I.; Kovalyuk, Z.D. Two-dimensionalization of electron gas in n-InSe crystals induced by electron irradiation. *Acta Phys. Pol. A* **2020**, *137*, 1031–1036. [CrossRef]
40. Emel'yanenko, O.V.; Lagunova, T.S.; Nasledov, D.N.; Talalkin, G.N. Formation and properties of impurity band in n-GaAs. *Sov. Phys. Solid State* **1965**, *7*, 1063–1070. [CrossRef]
41. Kress-Rogers, E.; Nicholas, R.J.; Portal, J.C.; Chevy, A. Cyclotron resonance studies on bulk and two-dimensional conduction electrons in InSe. *Solid State Communs.* **1982**, *44*, 379–383. [CrossRef]
42. Riera, J.; Segura, A.; Chevy, A. Transport properties of silicon doped *n*-indium selenide. *Appl. Phys. A* **1992**, *54*, 428–430. [CrossRef]